



## Correlation between damage evolution, structural and optical properties of Xe implanted CrN thin films

Maja Popović<sup>1,\*</sup>, Mirjana Novaković<sup>1</sup>, Kun Zhang<sup>2</sup>, Miodrag Mitrić<sup>1</sup>, Nataša Bibić<sup>1</sup>, Zlatko Rakočević<sup>1</sup>

<sup>1</sup>University of Belgrade, Vinča Institute of Nuclear Sciences, 11321 Belgrade, Serbia

<sup>2</sup>Physikalisches Institut, Georg-August-Universität Göttingen, Friedrich-Hund-Platz 1, 37077 Göttingen, Germany

Received 3 April 2018; Received in revised form 22 May 2018; Accepted 16 June 2018

### Abstract

Polycrystalline CrN thin films were irradiated with Xe ions. The irradiation-induced modifications on structural and optical properties of the films were investigated. The CrN films were deposited on Si(100) wafers with the thickness of 280 nm, by using DC reactive sputtering. After deposition, the films were implanted at room temperature with 400 keV Xe ions with the fluences of  $5\text{--}20 \times 10^{15}$  ions/cm<sup>2</sup>. The films were then annealed at 700 °C in vacuum for 2 h. The combination of Rutherford backscattering spectrometry (RBS), X-ray diffraction (XRD) and transmission electron microscopy (TEM) was used for structural analyses, while changes in optical properties were monitored by spectroscopic ellipsometry. We also measured the electrical resistivity of the samples using a four point probe method. RBS analysis reveals that the concentration of Xe in the layers increases with ion fluence reaching the value of around 1.5 at.% for the highest ion dose, at a depth of 73 nm. XRD patterns show that the irradiation results in the decrease of the lattice constant in the range of 0.4160–0.4124 nm. Irradiation also results in the splitting of 200 line indicating the tetragonal distortion of CrN lattice. TEM studies demonstrate that after irradiation the columnar microstructure is partially destroyed within ~90 nm, introducing a large amount of damage in the CrN layers. Spectroscopic ellipsometry analysis shows that the optical band gap of CrN progressively reduces from 3.47 eV to 2.51 eV with the rise in ion fluence up to  $20 \times 10^{15}$  ions/cm<sup>2</sup>. Four point probe measurements of the films indicated that as the Xe ion fluence increases, the electrical resistivity rises from 770 to 1607  $\mu\Omega\text{cm}$ . After post-implantation annealing crystalline grains become larger and lattice distortion disappears, which influences optical band gap values and electrical resistivity of CrN.

**Keywords:** CrN, thin films, XRD, ellipsometry, optical band gap

### I. Introduction

Due to their excellent mechanical properties, transition metal nitrides are widely used as protective coatings in industrial applications. Among them chromium nitride (CrN) has attractive combination of desirable physical, chemical and mechanical characteristics [1]. These remarkable characteristics such as high hardness (22–25 GPa), high wear- and corrosion resistance, low friction coefficient make it attractive for cutting tools and wear application, as diffusion barriers in the field of nano-electronics, and as corrosion and abrasion-

resistant coatings on optical and mechanical components [2–4]. On the other hand, the CrN is also interesting due to its magnetic, optical and electronic properties, after being reported as a semiconductor material in the recent studies [5].

To improve physical, chemical and mechanical properties of thin films, the different treatments can be used such as doping, annealing, ion implantation, plasma treatment, etc. [6–11]. Among them ion implantation as a non-thermal and non-equilibrium technique possesses a series of advantages including accurate control of the ion concentration-depth distribution, incorporation of almost all elements in different systems conducted at room temperature thus offering interesting possibilities.

\*Corresponding authors: tel/fax: +381 11 6308 425, e-mail: [majap@vinca.rs](mailto:majap@vinca.rs)

Since defect formation is associated with ion implantation, lattice disorder will be produced and consequently the properties of the systems will be changed. In the case of CrN thin films, ion implantation has already been used in the modification of structural, mechanical and optoelectronic properties. Experimental results have shown that the implantation of keV Nb ions in polycrystalline CrN films can effectively enhance the hardness of the films [6]. Ag and Au irradiations show changes in optical properties due to the formation of silver and gold nanoparticles and the excitation of surface plasmon resonance in the visible region of the spectra [12,13], Ar ions irradiation results in the structural changes and progressive reduction of optical band gap of CrN films [11]. In addition, implanted xenon ions are known to form aggregates and bubbles in various materials such as Si<sub>3</sub>N<sub>4</sub> [14], silicon [15], ZrC [16], graphite [17], aluminium [18], inducing swelling and cracks due to its low solubility. It was found that due to xenon's chemical inertness and relatively large atomic number the reaction process in the material can be simply described by as formation of the physical damage. Thus, a successful application of Xe ion implantation depends on understanding the production of damage in the film.

The goal of this study was to determine changes of the structural and optical properties of CrN thin films after 400 keV Xe ions implantation. These changes were investigated on the basis of irradiation damage formation and performed post-implantation annealing. Optical properties in conjunction with the structural parameters, such as lattice constant and crystallite size are discussed. An attempt was made to clarify whether the optical properties of the CrN layers could be controlled by combining ion irradiation and thermal annealing. It was shown that observed changes in optical band gap of CrN films can be directly correlated with the variation in crystallite size and damage induced by the irradiation of the films. The structural changes are also correlated to the measured electrical resistivity.

## II. Experimental

### 2.1. Sample preparation

Polycrystalline CrN films with thickness of 280 nm were deposited by DC reactive sputtering in a commercial Bulzers Sputtron II system, using 1.5 keV argon ions and 99.9% pure Cr target. The chamber was evacuated to  $1 \times 10^{-4}$  Pa, while the argon and nitrogen partial pressures were  $1 \times 10^{-1}$  Pa and  $5 \times 10^{-2}$  Pa, respectively. The substrates used were 550  $\mu$ m thick Si(100) wafers, which were cleaned in diluted hydrofluoric acid and deionized water, and kept at 150 °C during deposition. Experimental parameters were chosen so that the deposition rate at the substrate was  $\sim 11$  nm/min. The CrN thin films were subsequently implanted with singly charged Xe ions with an ion energy of 400 keV by means of the Göttingen IONAS implanter [19]. The irradiations were performed at room temperature with

ion fluences of 5, 10, 15 and  $20 \times 10^{15}$  ions/cm<sup>2</sup>. During irradiation at a base pressure of about  $1 \times 10^{-6}$  Pa in the implantation chamber, typically 2–3  $\mu$ A xenon ion beam was scanned homogeneously over the full  $10 \times 10$  mm<sup>2</sup> surface of the samples by means of an electric *xy*-scanning device. The irradiation process was simulated by SRIM2011 program [20]. The implantation energy was chosen in such a way that all ions are stopped inside CrN layer. According to the simulation the implantation profile of 400 keV Xe in CrN has a mean range of  $R_p = 75$  nm and a full width at half maximum of  $\Delta R_p = 24$  nm. Un-irradiated and all Xe-irradiated samples were annealed in vacuum for 2 hours at temperature of 700 °C. The pressure inside the furnace was kept around  $10^{-6}$  Pa during annealing.

### 2.2. Characterization techniques

The structural and optical characterizations of CrN thin samples irradiated with 400 keV Xe ions and annealed at 700 °C were done by Rutherford backscattering spectrometry (RBS), X-ray diffraction (XRD), transmission electron microscopy (TEM) and spectroscopic ellipsometry. For studying the electrical properties of the films four probe method was used.

Depth profiling of CrN films was performed by 900 keV He<sup>++</sup> ion beam provided by the Göttingen IONAS implanter [19]. RBS spectra were taken with two silicon surface barrier detectors mounted at  $\pm 165^\circ$  with respect to the beam, having an energy resolution of 13 keV FWHM. The software used in simulation of RBS spectra was WiNDF code [21].

The XRD patterns of the samples were recorded using PHILIPS PW1050 diffractometer with monochromatized CuK $\alpha$  radiation ( $\lambda = 0.15418$  nm) in Bragg-Brentano geometry. The XRD spectra were collected in a  $2\theta$  scan range of 35–47° with a step size of 0.01° and an integration time of 0.5 s. Phase identification of the films was confirmed by matching the diffraction peaks with those of JCPDS database.

The characterization of the CrN films by transmission electron microscopy in cross-section, was carried out by using PHILIPS CM30 microscope, operated at 300 keV voltage. The samples for TEM examination were prepared by conventional procedure including cutting and mounting of the samples onto copper slot, followed by polishing and Ar ions milling. In addition, micro-diffraction (MD) technique was used for studying the crystalline structure of the films.

The optical properties were characterized by using HORIBA-Jobin Yvon UVIS ellipsometer over the spectral range from 260 to 2066 nm. The spectra were recorded digitally using Delta Psi2 software, with a 0.1 eV intervals and a collection time of 200 ms per each point. The measurements were taken using 1 mm spot size under an incident angle of 70° with respect to the surface normal.

Sheet resistance of the samples was measured with a JANDEL RM 3000 Universal probe. The values were

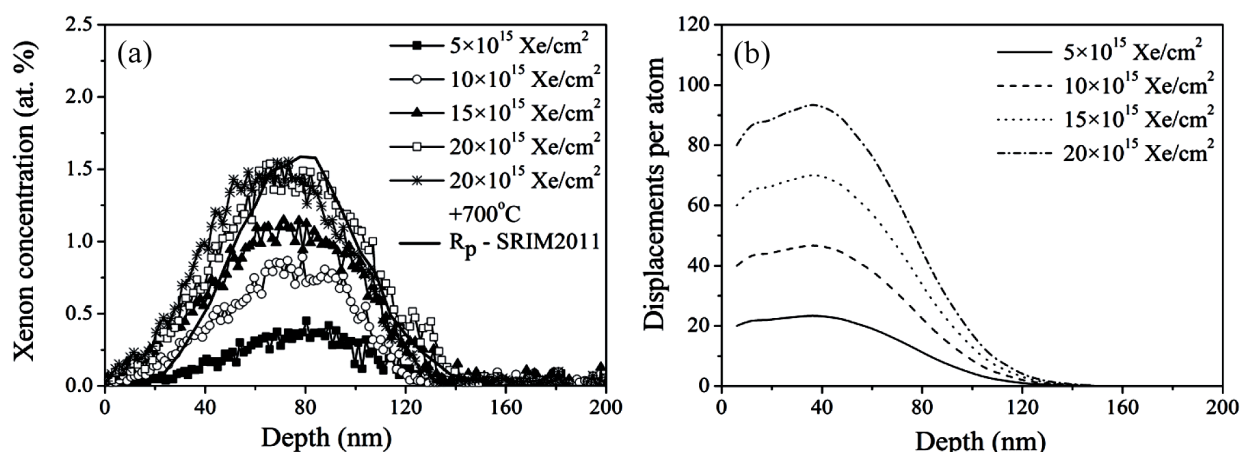


Figure 1. (a) Xe concentration depth profiles of CrN samples irradiated with different doses deduced by means of WiNDF code from the RBS spectra together with SRIM2011 calculation. The sample irradiated with  $20 \times 10^{15}$  ions/cm<sup>2</sup> was measured and analysed again after annealing for 2 h at 700 °C. (b) SRIM simulation of DPA value of 400 keV Xe ions irradiation on CrN films

calculated as specific resistivity to compare the results.

### III. Results and discussion

#### 3.1. Xe distribution in CrN films

Compositional analysis done by RBS has shown that the as deposited CrN films obtained under the given deposition conditions have stoichiometry close to Cr : N = 1 : 1 [22]. The concentration profiles of implanted Xe calculated from the experimental RBS spectra using the ion beam analysis computer code WiNDF are presented in Fig. 1a. The calculated spectra show that the maximum depth of xenon is up to 140 nm beneath the surface. As expected, the linear increase in the concentration of Xe ions with the rise in the ion fluence is observed. A maximum Xe concentration of about 1.5 at.% can be found in a depth of approximately 73 nm for the highest ion fluence. Also, with increasing ion fluence the position of the maximum was slightly shifted towards the surface which can be easily attributed to the concurrent sputtering which took place during ion irradiation. These experimentally obtained depth distributions are in agreement with the theoretically evaluated projected ion range of  $R_p \pm \Delta R_p = 75 \pm 24$  nm calculated by SRIM2011 program [20]. The Xe profile extracted from the spectrum taken from the sample implanted with the highest ion fluence and annealed 2 h at 700 °C is also included in Fig. 1a. As it can be observed, annealing of the sample further shifts the Xe profile to the surface. In particular, the maximum Xe concentration is slightly lower as compared to the as-implanted sample, which is most probably result of Xe atom diffusion out of the sample due to the high-temperature annealing. Similar behaviour was already reported in the previous study for argon implanted CrN layers annealed at 700 °C [11].

The SRIM simulated damage events of CrN films introduced by Xe ions irradiation are illustrated in Fig. 1b. As it is shown, the calculated DPA (displacements per atom) for the fluences of 5, 10, 15 and  $20 \times 10^{15}$  ions/cm<sup>2</sup>

was yielded to be 23, 47, 70 and 94, respectively. The calculations were achieved with K-P quick calculation and the DPAs were obtained using the *vacancy.txt* file. The simulation suggests that the Xe ions with their large atomic number can introduce a large damage inside 130 nm of the films with the maximum at around 35 nm. To our knowledge Xe behaviour in CrN is not examined experimentally. But, a few studies have been carried out on other transition metal-nitrides, such as TiN, influenced by Xe ions irradiation [23–25]. The authors in these reports found that the Xe ions produce a great damage in this kind of systems. Moreover, our recent experiments on the CrN system give evidence that the damage was produced along the ion track even after implantation with much lighter inert Ar ions [11,22].

#### 3.2. XRD analysis of CrN films

Our previous study [22] showed that the as-deposited CrN thin film has a polycrystalline structure with the crystallites aligned preferentially along (200) plane. XRD patterns of the as deposited CrN film and films irradiated with xenon ions at fluences of  $5 \times 10^{15}$  ions/cm<sup>2</sup> and  $20 \times 10^{15}$  ions/cm<sup>2</sup> are shown in Fig. 2. Also, in Fig. 2 the patterns taken on the samples implanted with the fluence of  $5 \times 10^{15}$  ions/cm<sup>2</sup> and  $20 \times 10^{15}$  ions/cm<sup>2</sup>, annealed 2 h at 700 °C are plotted. The presented spectral range was restricted to the region of  $2\theta = 35\text{--}47^\circ$ , where the changes were observed most clearly. Two peaks at  $37.44^\circ$  and  $43.67^\circ$  corresponding to the 111 and 200 lines of CrN cubic structure (*Fm3m*) are detected in the as deposited film, giving a lattice parameter  $a = 0.4160$  nm. This value is very close to the value given by the JCPDS No. 00-011-0065 [26]. After implantation with the fluence of  $5 \times 10^{15}$  ions/cm<sup>2</sup>, the crystallographic cubic structure is preserved; the primary phase of the Xe-ion implanted films includes CrN 111 and CrN 200 lines, which are nearly identical to that of unimplanted CrN. It was found that after implantation the diffraction peaks shift to higher  $2\theta$  angles. Calculated from XRD data, the lattice constant of the Xe-ion im-

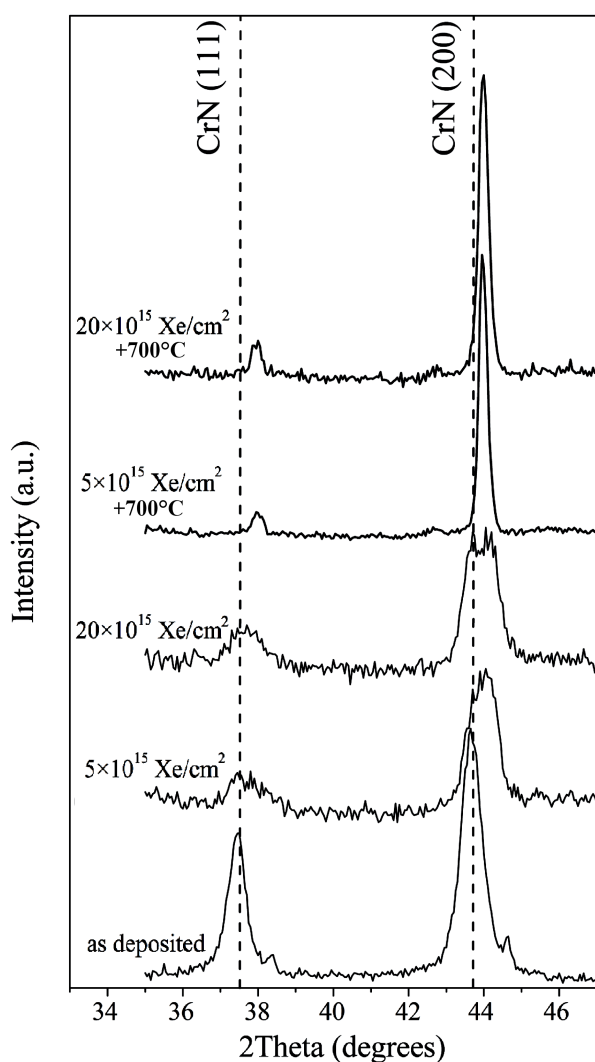


**Figure 2.** XRD diffraction patterns of prepared CrN samples (dashed lines correspond to the reference values of CrN [26])

planted CrN film is  $a = 0.4133$  nm, which is smaller than that of the as-deposited, hence resulting in approximately 1% of the lattice contraction. With further increase of ion fluence the peaks continue to shift, giving a slight decrease of lattice parameter to 0.4124 nm. The shifting nature of diffraction peaks in polycrystalline films after irradiation is believed to be associated with the build up of stress in CrN and change of its interplanar spacing, which arise from the creation of high amount of defects in the films.

**Table 1.** XRD analysis of the as-deposited and ion-implanted CrN samples (diffraction angle  $2\theta$ , interplanar spacing  $d$ , lattice constant  $a$  and mean grain size  $D$ )

Sample	(111) $2\theta$	(200) $2\theta_1/2\theta_2$	$d$ [nm]	$a$ [nm]	$D$ [nm]
As-deposited	37.4368	43.6732	0.2402	0.4160	14.5
$5 \times 10^{15}$ Xe/cm <sup>2</sup>	37.6546	43.7225/44.1446	0.2389	0.4133	14.1
$20 \times 10^{15}$ Xe/cm <sup>2</sup>	37.7059	43.6786/44.1856	0.2386	0.4124	14.0
$5 \times 10^{15}$ Xe/cm <sup>2</sup> + 700 °C	37.9847	43.9802	0.2387	0.4103	26.5
$20 \times 10^{15}$ Xe/cm <sup>2</sup> + 700 °C	37.9558	43.9915	0.2370	0.4100	30.6

Another aspect of the possible influence of the ion irradiation is on the variation in the shape of diffraction lines. The splitting of 200 line is clearly observed, which is otherwise not present in 111 diffraction peak. This is an indication of the tetragonal distortion of CrN lattice induced by the implantation of Xe ions. The observed diffraction peak splitting has never been examined and reported in the literature for xenon ions implantation in CrN layers. In order to analyse the splitting, the 200 line was fitted with two peaks ( $2\theta_1$  and  $2\theta_2$ ) using the Koalariet computing program based on Fundamental parameters convolution approach to generate line profiles [27]. The splitting is more pronounced with increasing ion fluence, which is expected since an inert xenon ions do not react with any elements in CrN, but produce crystal defects with high rate resulting in the damaged structure along the ion track. These defects generate additional stress in the lattice, thus provoking a change in the lattice parameters for the irradiated samples. As indicated by the SRIM simulation, the as-produced DPA yields the value up to 94, which thus will impact the structure of the films. Note also the observed broadening of 111 and 200 diffraction peaks in CrN after Xe ions irradiation, which is probably due to the damage induced microstrain in the cell, already reported in literature [22,28]. The broadening of XRD lines is an indication of the formation of smaller grains. Indeed, the crystallite size was calculated [27], and it was found that the xenon ions led to the formation of slightly smaller grains.

In the patterns taken on the  $5 \times 10^{15}$  ions/cm<sup>2</sup> and  $20 \times 10^{15}$  ions/cm<sup>2</sup> post-annealed samples (Figs. 2), the peaks 111 and 200, belonging to CrN, are also clearly identified without trace of any other phases. It can be seen that after annealing there is no distortion of 200 line, the peak is narrow and much more intense as compared to as-implanted samples. It is implied that the peak narrowing behaviour could possibly originate from the grain growth and the annihilation of defects during annealing at high temperature. The estimated crystallite size increases after annealing to around 30 nm. The values of peaks position, lattice constant, interplanar spacing and mean grain size calculated from the different spectra are summarized in Table 1.

### 3.3. TEM observations on CrN films

In previous experiments [22], the investigated CrN layers were found to grow in the form of columnar structure, typical for sputter deposited metal-nitrides [29,30].

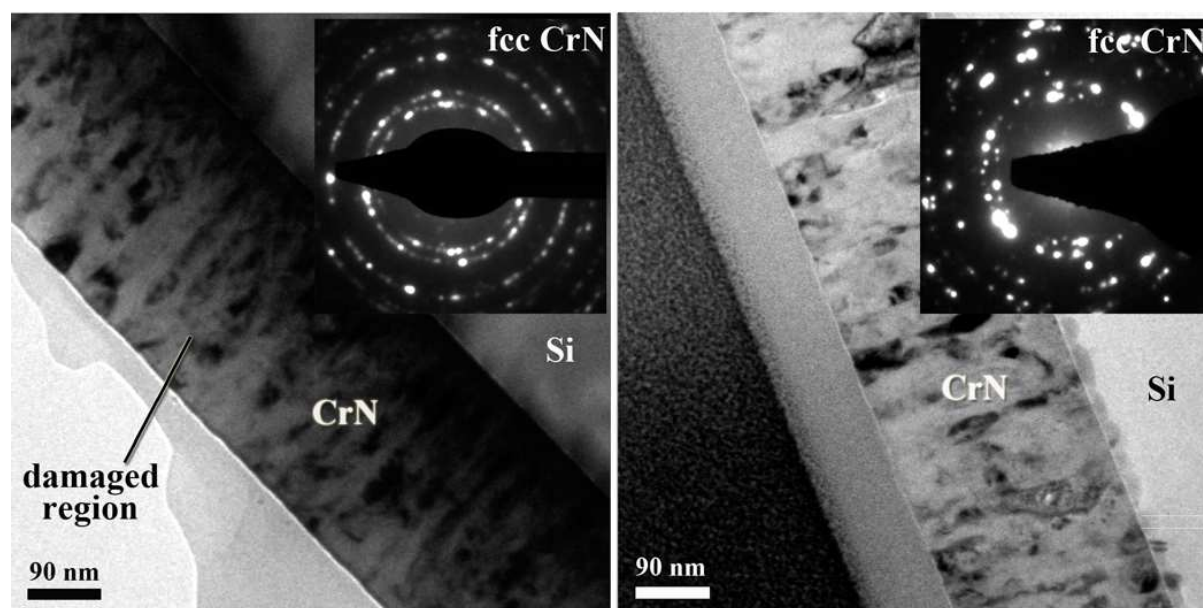


**Figure 3. Bright-field cross-sectional TEM image of CrN film implanted with the fluence of  $20 \times 10^{15}$  Xe/cm<sup>2</sup> before (a) and after annealing at 700 °C (b) and corresponding MD diffraction patterns**

In Figs. 3a and 3b bright field cross-sectional TEM images of CrN sample implanted with the highest ion fluence of  $20 \times 10^{15}$  ions/cm<sup>2</sup> before and after annealing in vacuum 2 h at 700 °C were presented. The corresponding MD patterns were taken in the same cross-sectional view, covering a layer, without underlying Si substrate and shown in the upper right part of the corresponding image. In as-implanted sample (Fig. 3a) the destroyed columnar structure is clearly observed. Similar behaviour was observed with the CrN samples implanted with chromium ions, which was also investigated via TEM [31]. These structural changes appear to be the most pronounced within 90 nm of the layer, where the highest amount of energy is deposited in the collision processes, while the part of the layer towards the substrate remains practically unaffected. Diffraction rings in the MD pattern identify isolated *fcc* CrN phase with very fine nanocrystalline grains indicating that the polycrystalline structure is retained after irradiation. Subsequent vacuum annealing of this implanted sample (Fig. 3b) affects the structure of the layer. A closer analysis shows that individual crystal grains grow much larger upon heat treatment [11]. MD pattern in this case still corresponds to *fcc* CrN phase. Isolated bright spots on diffraction rings become sharper and bigger indicating the formation of larger grains due to the grain coalescence effect developed after 700 °C. This is in agreement with XRD findings according to which the grains become as large as ~30 nm (see Table 1).

### 3.4. Optical characterization

The influence of implanted Xe ions on the optical properties of CrN thin films is studied using spectroscopic ellipsometry. Detailed information about optical parameters such as refractive index *n*, and extinction coefficient *k*, were obtained using an appropriate model in

fitting the experimental  $\psi$  and  $\Delta$  spectra. Good agreement obtained between measured and calculated ellipsometric spectra indicates that the model used in the analysis is convenient and that the calculated results are reliable. The description of the model used in the fitting of experimental CrN spectra was described in detail in literature [11]. Figure 4 shows *n* and *k* spectra over the photon energy of 0.6–4.8 eV for CrN thin films implanted with different Xe ion fluences and subsequently annealed at 700 °C, respectively. The spectrum of the as deposited film is also given for comparison with the spectra of the implanted films. We can notice that the as deposited film exhibits maximum values of refractive index in the low energy part of the spectrum and almost exponential decrease with increasing photon energy up to ultraviolet region (Fig. 4a). The optical constant *n* of our CrN layer quite well match with the one reported by Aouadi *et al.* [32]. After Xe ion implantation the intensity of the refractive index is changed while the slope of the curves remains the same. The *n* values decrease with Xe ions and the change is most visible for the fluence of  $10 \times 10^{15}$  ions/cm<sup>2</sup>. The refractive index dependence, in turn, is a consequence of changes in the structure that increase with the number of implanted ions. The more implanted ions there are, the more defects exist, which lowers the refractive index. During the Xe ion implantation complex interactions between high energy particles and target atoms occur, which lead to deformation of the lattice in the films as previously shown in XRD analysis. As for the extinction coefficient it was found that *k* values for the as deposited sample increases with photon energy up to 2.0 eV, while decreases for higher energy values [32]. After Xe ions irradiation the shape of the extinction coefficient curves was changed. It can be seen that the *k* parameter is much more sensitive to the variation of irradiation fluence at lower photon en-

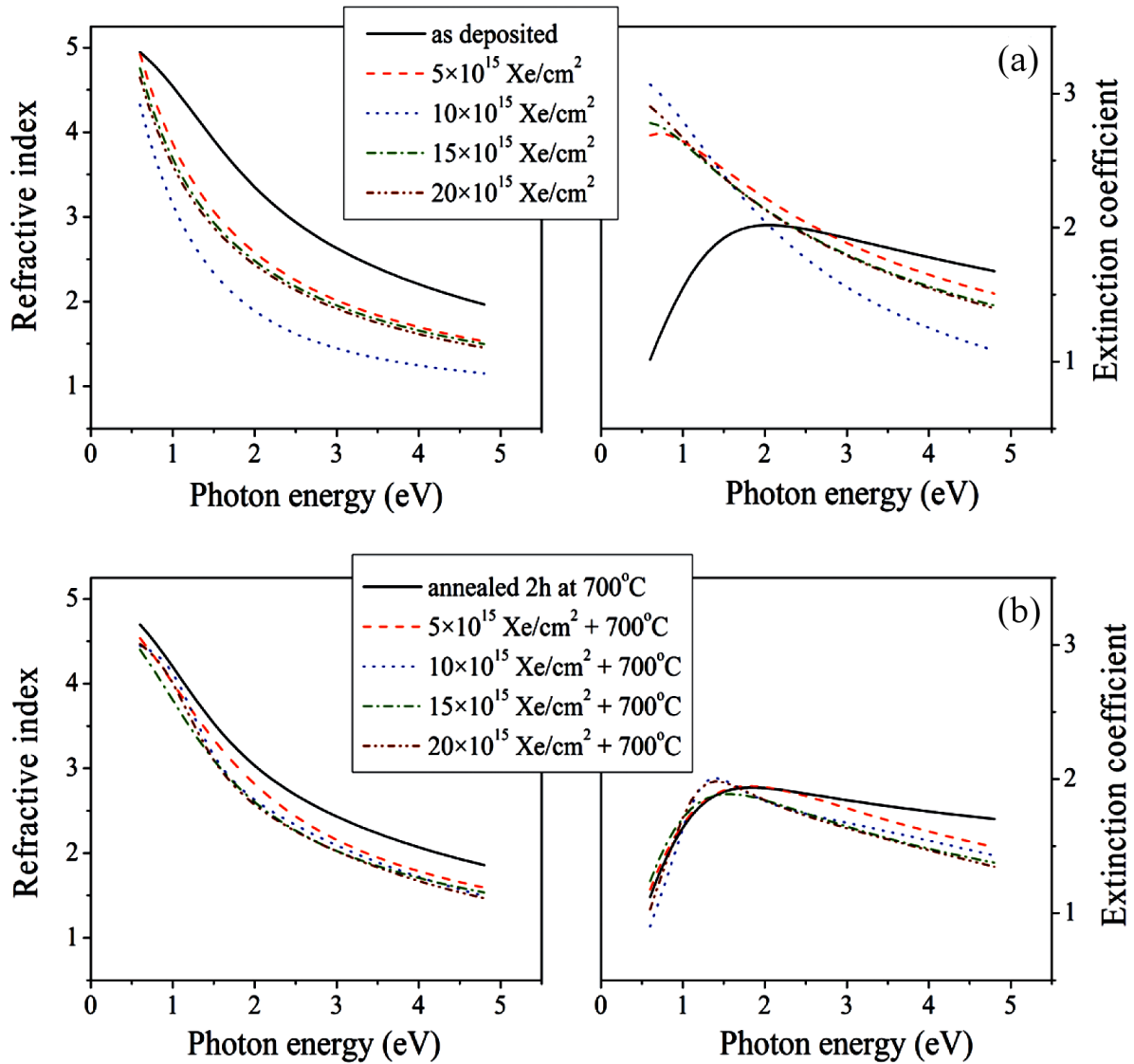


Figure 4. Refractive index  $n$  and extinction coefficient  $k$ -spectra as a function of photon energy for Xe ion implanted CrN films (a) and subsequently annealed at 700 °C (b)

ergies, exhibiting notably higher values as compared to the as deposited sample. On the other hand, subsequent annealing of implanted samples did not significantly change the optical constants (Fig. 4b). The refractive index and extinction coefficient curves show very similar shape as in the case of the as deposited sample, with slightly smaller absolute values, indicating that the defect concentration as well as crystallographic structure did not notably changed after the post-irradiation heat treatment.

From the extinction coefficient spectra the energy profiles of the absorption coefficient,  $\alpha$ , have been derived ( $\alpha = 4\pi k/\lambda$ ) and shown in Fig. 5 for the Xe implanted CrN films and subsequently annealed at 700 °C. The spectrum of the as deposited sample (Fig. 5a) shows the usual minimum absorption in the low energy region and exponential increase with increasing photon energy. The presence of Xe ions changes the slope of absorption curves: as compared to the as deposited sam-

ple, higher absorption in the low energy region was observed, while Xe ions induce a decrease of absorption coefficient above the photon energy of 2.5 eV. These changes could be attributed to the production of defect levels in the band gap and/or to the increase of the carrier concentration during irradiation or production of metallic Cr clusters due to the loss of nitrogen atoms. Similar effects were already observed for CrN films implanted with Ar ions [11]. After annealing at 700 °C (Fig. 5b) the absorption coefficient did not change for the photon energies lower than 2 eV, and beyond this energy value it starts to decrease.

Significant parameter that characterizes semiconductor and dielectric materials is the optical band gap energy ( $E_g$ ) which presents very important property in the design and modelling of optical devices. The band gap energies of Xe implanted and also post-annealed CrN films are calculated using the following Tauc relationship [33]:

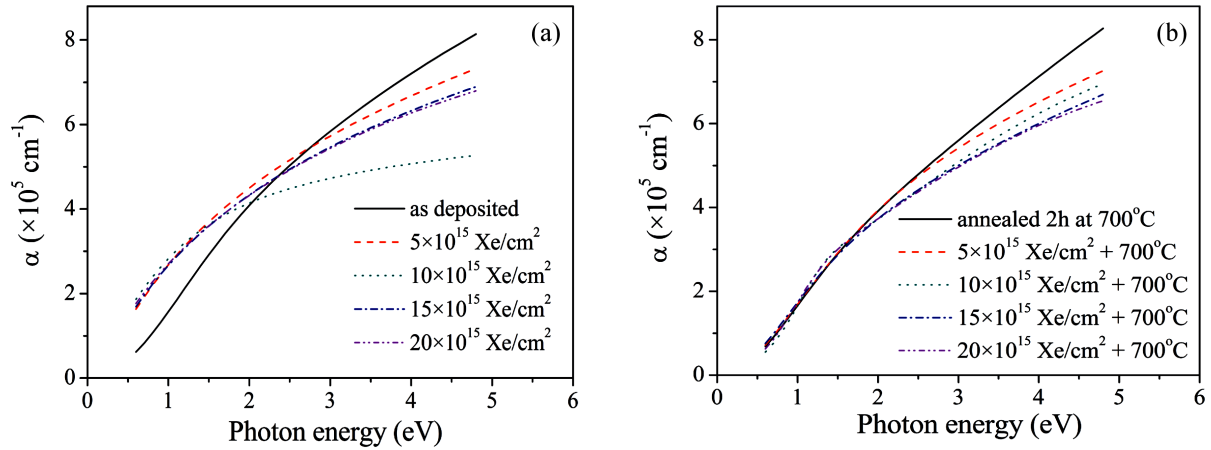


Figure 5. Absorption coefficients of CrN thin films irradiated with different Xe ion fluences (a) and post-annealed at 700 °C (b)

Table 2. Band gap values ( $E_g$ ) of as-deposited, Xe ion irradiated and annealed CrN layers

Dose/Treatment	Band gap energy, $E_g$ [eV]				
	0	$5 \times 10^{15}$ ions/cm <sup>2</sup>	$10 \times 10^{15}$ ions/cm <sup>2</sup>	$15 \times 10^{15}$ ions/cm <sup>2</sup>	$20 \times 10^{15}$ ions/cm <sup>2</sup>
Xe irradiated	3.47	3.05	2.92	2.77	2.51
Xe irradiated + 700 °C	3.09	3.08	3.05	3.02	3.00

$$\alpha \cdot h \cdot \nu = A(h \cdot \nu - E_g)^{1/2} \quad (1)$$

where  $A$  is a constant,  $\nu$  is the frequency of the incident light and  $h$  is the Plank constant. Since  $E_g = h\nu$  when  $(\alpha h\nu)^2 = 0$ , an extrapolation of the linear region of the plot of  $(\alpha h\nu)^2$  versus photon energy ( $h\nu$ ) on the  $x$ -axis gives the value of the optical band gap. Figure 6 shows the Tauc plots for the Xe irradiated and post-annealed CrN thin films. The variation of band gap energy with Xe ion fluence before and after annealing is presented in Fig. 7. The as deposited CrN film is found to have band gap energy of 3.47 eV which is slightly higher than the value of 3.4 eV reported by Fu *et al.* [34]. After Xe ions irradiation, this value decreases and shows a progressive reduction with increasing the irradiation fluence. The observed red shift could be explained on the basis of increasing the degree of disorder and

density of defects due to the addition of Xe ions into CrN films. Consequently, energy band gap data show that CrN film has the lowest value of 2.51 eV after implantation with the fluence of  $20 \times 10^{15}$  ions/cm<sup>2</sup>. It is believed that with the gradual increase of ion fluence the degree of implantation induced damage in the films is increased together with the monotonic decrease in their crystallinity. Hence, optical band gap decreases continuously with the increase of ion fluence. Similar behaviour was already observed in our previous report on 200 keV Ar ions implantation in CrN films [11]. Annealing at 700 °C does not have much effect on the band gap. A slightly decreasing trend was noticed. The band gap energy varies with increasing ion fluence in the very narrow range from 3.09 to 3.00 eV. The band gap values for all samples are summarized in Table 2. The band gap analyses of CrN films are overall well-consistent with XRD and TEM results.

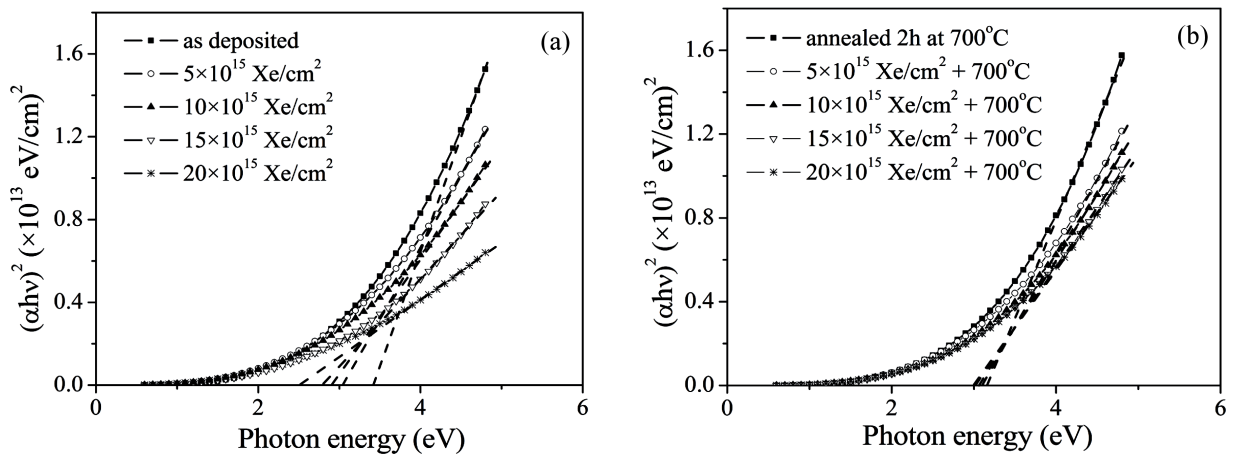


Figure 6. Optical band gap energy of Xe ion implanted CrN thin films: a) before and b) after annealing at 700 °C

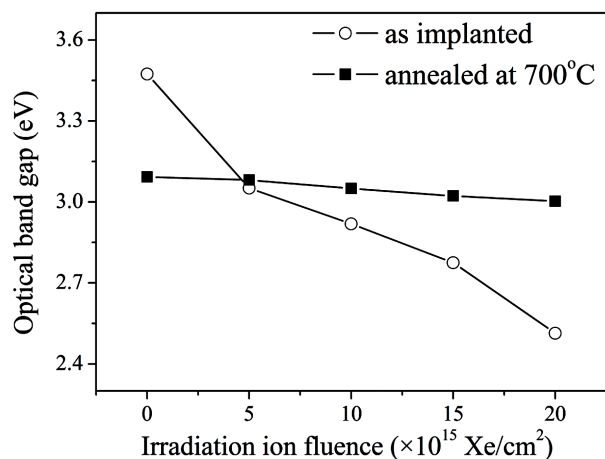


Figure 7. Dependence of optical band gap energy  $E_g$  of CrN films on the Xe ion fluence before and after annealing at 700 °C

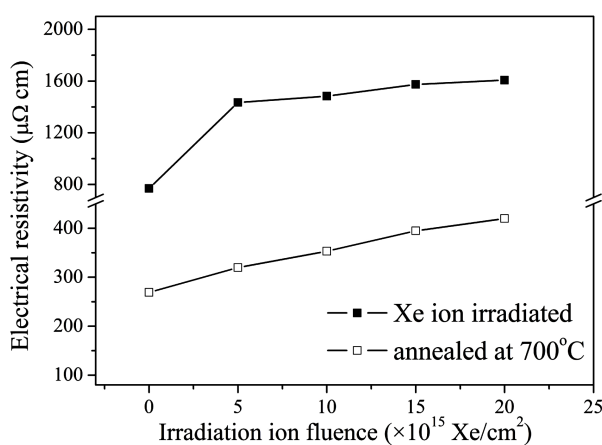


Figure 8. Electrical resistivity of CrN films irradiated with 400 keV xenon ions

### 3.5. Electrical resistivity measurements

In Fig. 8 the electrical resistivity of CrN samples implanted with Xe ions and annealed at 700 °C as a function of the irradiation fluence is plotted. The as deposited CrN film has a high resistivity of about 770  $\mu\Omega$ cm, which is 15% larger than the CrN bulk value. Such observations are in a good agreement with the work reported on CrN thin films fabricated by DC magnetron sputtering [35]. Upon Xe ion irradiation with  $5 \times 10^{15}$  ions/cm<sup>2</sup> the resistivity of CrN sample increases by a factor of 2, and continues to increase with an ion dose. Obviously, ion induced damage in the layer has a predominant role on metallic behaviour of CrN leading to an overall increase of electrical resistivity of CrN. These changes are much more pronounced in comparison with Ar implanted CrN films [36] due to higher energy of Xe ions and their larger atomic number which introduced considerable amounts of defects in the films. Having this in mind the resistivity of CrN can be easily changed in the wide range by varying Xe concentration in the layers. After annealing at 700 °C resistivity significantly decreased which can be attributed to the lower

concentration of different kinds of defects and also formation of larger crystallites at elevated temperatures.

## IV. Conclusions

In this paper, the structural and optical properties of the Xe modified CrN thin films were analysed as a function of the ion fluence and post-implantation annealing in vacuum. The XRD analysis revealed that upon xenon ions irradiation polycrystalline structure of the films was retained, while structural parameters were significantly affected resulting in a splitting of 200 line and contraction of the CrN lattice. The splitting is more pronounced with increasing ion fluence indicating tetragonal distortion of CrN lattice. The observed variation in structure can be attributed to the formation of the high density damage region in the CrN structure. TEM analysis found that this damage region is mainly distributed within ~90 nm from the surface of the CrN layer. Further, the optical property measurement implies that the optical band gap for the Xe irradiated samples decreases gradually with increasing ion fluence. It is a combined result of the decrease of crystallite size and damage induced by the irradiation. The optical band gap for post-annealed samples remains nearly constant with increasing ion fluence. This could be mainly attributed to the formation of bigger crystallites and reduction of defects at higher temperature. The observed changes are correlated with the variation of electrical resistivity of the layers. The changes of the structural and optical parameters with the increase of Xe irradiation fluence and after annealing at 700 °C have shown that the optical properties of CrN films are directly defined by the lattice disorder and hence can be tailored and controlled by combining ion irradiation and thermal annealing. The conclusions drawn in the present work suggest in which direction these studies could be possibly extended, namely a more systematic variation of ion fluences and annealing temperature over larger ranges.

**Acknowledgement:** This work was supported by the Ministry of Education and Science of the Republic of Serbia (Project No. III 45005). We would like to thank D. Purschke and P. Wilbrandt for their support during the experiments.

## References

1. R.F. Bunshah, *Handbook of Hard Coatings: Deposition Technologies, Properties and Applications*, Noyes Publication, Norwich, NY, 2001.
2. J. Lin, Z.L. Wu, X.H. Zhang, B. Mishra, J.J. Moore, W.D. Sproul, "A comparative study of CrNx coatings synthesized by dc and pulsed dc magnetron sputtering", *Thin Solid Films*, **517** (2009) 1887–1894.
3. S.H. Shin, M.W. Kim, M.C. Kang, K.H. Kim, D.H. Kwon, J.S. Kim, "Cutting performance of CrN and Cr-Si-N coated end-mill deposited by hybrid coating system for ultra-high speed micro machining", *Surf. Coat. Technol.*, **202** (2008) 5613–5616.

4. S.-H. Lee, T.-H. Yang, S.-H. Hyun, Y.-S. Yoon, “Corrosion behavior of pre-oxidized and thermally nitrated stainless steel for polymer electrolyte membrane fuel cell bipolar plates”, *Corros. Sci.*, **58** (2012) 79–85
5. D. Gall, C.S. Shin, R.T. Spila, M. Odén, M.J.H. Senna, J.E. Greene, I. Petrov, “Growth of single-crystal CrN on MgO(001): Effects of low-energy ion-irradiation on surface morphological evolution and physical properties”, *J. Appl. Phys.*, **91** (2002) 3589–3597.
6. Y.-Y. Chang, D.-Y. Wang, W. Wu, “Tribological enhancement of CrN coatings by niobium and carbon ion implantation”, *Surf. Coat. Technol.*, **177-178** (2004) 441–446.
7. K. Ibrahim, M. Mahbubur Rahman, X. Zhao, J.-P. Veder, Z.-F. Zhou, E. Mohammadpour, R.H. Majeed, A.N. Nikoloski, Z.-T. Jiang, “Annealing effects on microstructural, optical, and mechanical properties of sputtered CrN thin film coatings: Experimental studies and finite element modeling”, *J. Alloys Compd.*, **750** (2018) 451–464.
8. M. Mahbubur Rahman, Z.-T. Jiang, Z. Xie, X. Duan, Z.-f. Zhou, P.C. Wo, C.-Y. Yin, N. Mondinos, Q. Gu, H. Widjaja, K. Jack, A. Yago, A. Amri, “Understanding local bonding structures of Ni-doped chromium nitride coatings through synchrotron radiation NEXAFS spectroscopy”, *J. Phys. Chem. C*, **118** (2014) 18573–18579.
9. K. Ibrahim, M. Mahbubur Rahman, H. Taha, E. Mohammadpour, Z. Zhou, C.-Y. Yin, A. Nikoloski, Z.-T. Jiang, “Structural, morphological, and optical characterizations of Mo, CrN and Mo:CrN sputtered coatings for potential solar selective applications”, *Appl. Surf. Sci.*, **440** (2018) 1001–1010.
10. M. Mahbubur Rahman, Z.-T. Jiang, X. Duan, Z. Xie, A. Tadich, Z.-f. Zhou, N. Mondinos, C.-Y. Yin, M. Altarawneh, B.Z. Dlugogorski, “NEXAFS N K-edge study of the bonding structure on Al/Si doped sputtered CrN coatings”, *J. Alloys Compd.*, **661** (2016) 268–273.
11. M. Novaković, M. Popović, K. Zhang, Z. Rakočević, N. Bibić, “Effects of 200 keV Ar-ions irradiation on the structural and optical properties of reactively sputtered CrN films”, *Opt. Mater.*, **62** (2016) 57–63.
12. M. Novaković, M. Popović, E. Schmidt, P. Schöppe, M. Mitrić, N. Bibić, C. Ronning, Z. Rakočević, “Evolution of structural and optical properties of Ag implanted CrN thin films with annealing temperature”, *J. Alloys Compd.*, **729** (2017) 671–678.
13. M. Novaković, M. Popović, E. Schmidt, M. Mitrić, N. Bibić, Z. Rakočević, C. Ronning, “Clustering of gold particles in Au implanted CrN thin films: The effect on the SPR peak position”, *Appl. Surf. Sci.*, **426** (2017) 667–673.
14. Y.-U. Heo, M. Takeguchi, K. Mitsuishi, M. Song, Y. Nakayama, K. Furuya, “Precipitation behavior of Xe at grain boundaries in Si<sub>3</sub>N<sub>4</sub> ceramic during implantation at elevated temperature”, *J. Nucl. Mater.*, **397** (2010) 122–127.
15. G. Faraci, A.R. Pennisi, F. Zontone, “Fine structure effects and phase transition of Xe nanocrystals in Si”, *Eur. Phys. J. B*, **51** (2006) 209–213.
16. G. Gutierrez, N. Toulhoat, N. Moncoffre, Y. Pison, A. Maître, M. Gendre, A. Perrat-Mabillon, “Thermal behavior of xenon in zirconium carbide at high temperature: Role of residual zirconia and free carbon”, *J. Nucl. Mater.*, **416** (2011) 94–98.
17. R.G. Lacerda, M.C. Dos Santos, L.R. Tessler, P. Hammer, F. Alvarez, F.C. Marques, “Pressure-induced physical changes of noble gases implanted in highly stressed amorphous carbon films”, *Phys. Rev. B: Condens. Matter*, **68** (2003) 054104.
18. R.S. Dhaka, C. Biswas, A.K. Shukla, S.R. Barman, “Xe and Ar nanobubbles in Al studied by photoemission spectroscopy”, *Phys. Rev. B: Condens. Matter*, **77** (2008) 104119.
19. M. Uhrmacher, K. Pampus, F.J. Bergmeister, D. Purschke, K.P. Lieb, “Energy calibration of the 500 kV heavy ion implanter ionas”, *Nucl. Instrum. Meth. B*, **9** (1985) 234–242.
20. J.F. Ziegler, J.P. Biersack, U. Littmark, *The Stopping and Range of Ions in Solids*, Pergamon Press, New York, 1985.
21. N.P. Barradas, C. Jeaynes, R.P. Webb, “Simulated annealing analysis of Rutherford backscattering data”, *Appl. Phys. Lett.*, **71** (1997) 291–293.
22. M. Novaković, M. Popović, N. Bibić, “Ion-beam irradiation effects on reactively sputtered CrN thin films”, *Nucl. Instrum. Meth. B*, **268** (2010) 2883–2887.
23. M. Popović, M. Novaković, M. Mitrić, K. Zhang, Z. Rakočević, N. Bibić, “Xenon implantation effects on the structural and optical properties of reactively sputtered titanium nitride thin films”, *Mater. Res. Bull.*, **91** (2017) 36–41.
24. S. Gavarini, N. Toulhoat, C. Peaucelle, P. Martin, J. Mende, Y. Pison, H. Jaffrezic, “Xenon migration behaviour in titanium nitride”, *J. Nucl. Mater.*, **362** (2007) 364–373.
25. R. Bès, C. Gaillard, N. Millard-Pinard, S. Gavarini, P. Martin, S. Cardinal, C. Esnouf, A. Malchère, A. Perrat-Mabillon, “Xenon behavior in TiN: A coupled XAS/TEM study”, *J. Nucl. Mater.*, **434** (2013) 56–64.
26. Z.G. Pinsker, L.N. Abrosimova, *Kristallografiya*, **3** (1958) 281.
27. R.W. Cheary, A. Coelho, “A fundamental parameters approach to X-ray line-profile fitting”, *J. Appl. Crystallogr.*, **25** (1992) 109–121.
28. M. Novaković, M. Popović, N. Bibić, “Ion-beam irradiation effects on reactively sputtered CrN layers”, *Process. Appl. Ceram.*, **5** [1] (2011) 25–29.
29. A.P. Ehasarian, W.-D. Münz, L. Hultman, U. Helmersson, I. Petrov, “High power pulsed magnetron sputtered CrN<sub>x</sub> films”, *Surf. Coat. Technol.*, **163** (164) (2003) 267–272.
30. M. Popović, M. Novaković, N. Bibić, “Annealing effects on the properties of TiN thin films”, *Process. Appl. Ceram.*, **9** [2] (2015) 67–71.
31. S. Han, H.-Y. Chen, K.-L. Chang, K.-W. Weng, D.-Y. Wang, F.-H. Lub, H.C. Shih, “Effects of MEVVA-implanted chromium on the structure and properties of CrN film”, *Thin Solid Films*, **447-448** (2004) 425–429.
32. S.M. Aouadi, D.M. Mihut, M.L. Kuruppu, S.R. Kirkpatrick, S.L. Rohde, “Spectroscopic ellipsometry measurements of chromium nitride coatings”, *J. Vac. Sci. Technol. A*, **19** (2001) 2800–2804.
33. J.C. Tauc, *Optical Properties of Solids*, North-Holland, Amsterdam, 1972.
34. Y. Fu, M. Hou, G. Lin, J. Hou, Z. Shao, B. Yi, “Coated 316L stainless steel with Cr<sub>x</sub>N film as bipolar plate for PEMFC prepared by pulsed bias arc ion plating”, *J. Power Sources*, **176** (2008) 282–286.
35. B. Subramanian, K. Prabakaran, M. Jayachandran, “Influence of nitrogen flow rates on materials properties of CrN<sub>x</sub> films grown by reactive magnetron sputtering”, *Bull.*

- Mater. Sci.*, **35** (2012) 505–511.
36. M. Novaković, M. Popović, D. Peruško, V. Milinović, I. Radović, N. Bibić, M. Mitrić, M. Milinović, “Ion implantation induced structural changes in reactively sputtered Cr-N layers on Si substrates”, *Nucl. Instrum. Meth. B*, **257** (2007) 782–785.